Rheology of colloidal microphases in a model with competing interactions

Alessandra Imperio
Sezione dell'Università degli Studi di Milano, CNISM, Milano, Italy

Luciano Reatto
Dipartimento di Fisica, Università degli Studi di Milano, via Celoria 16, 20133 Milano, Italy

Stefano Zapperi
INFM-CNR, S3, Dipartimento di Fisica, Università di Modena e Reggio Emilia, via Campi 213/A, I-41100, Modena, Italy and ISI Foundation, Viale San Severo 65, 10133 Torino, Italy

(Received 7 February 2008; revised manuscript received 23 May 2008; published 4 August 2008)

We study the rheological properties of colloidal microphases in two dimensions simulating a model of colloidal particles with competing interactions. Due to the competition between short-range attraction and long-range repulsion, as a function of the density the model exhibits a variety of microphases such as clusters, stripes, or crystals with bubbles. We prepare the system in a confined microphase employing Monte Carlo simulations and then shear the resulting configurations by applying a drag force profile. We integrate numerically the equation of motion for the particles and analyze the dynamics as a function of the density and the applied strain rate. We measure the stress-strain curves and characterize the yielding of the colloidal microphases. The results depend on the type of microphase. (i) Clusters are easily sheared along layers and the relative motion is assisted by rotations. (ii) Stripes shear easily when they are parallel to the flow and tend to jam when they are perpendicular to it. Under a sufficiently strong shear rate perpendicular stripes orient in the flow direction. (iii) Crystals with bubbles yield by fracturing along the bubbles and eventually forming stripes. We discuss the role of dislocations, emitted by the bubbles, in the yielding process. Finally, we analyze the effect of thermal fluctuations on the rheological properties.

DOI: 10.1103/PhysRevE.78.021402 PACS number(s): 82.70.−y, 47.57.J−

I. INTRODUCTION

Examples of spontaneous pattern formation or microseparation, in conditions close to thermodynamic equilibrium, can be found in many different experimental systems, both in two [1–5] and in three dimensions [6–9]. The interest in these novel phases of matter is very high because the skill in controlling the architecture of particle aggregates, as well as the superstructures the latter arrange on, is nowadays a strategic tool in nanotechnology, in order to engineer new materials with specific electric, magnetic, optical, and rheological properties.

The topic of pattern formation is important not only from a technological point of view, but also from a fundamental one, influencing many different branches of science: from vitrification and gelation [10–13] to colloidal systems [14–17], from biological membranes [18] to network formation of tissue cells [19], to physisorbed layers on solid surfaces [20,21]. Even though all of these systems are rather different at the molecular level, the patterns formed by the particles can be similar: circular clusters, stripes, and rings of particles can be easily observed in most bidimensional systems, while lamellae, spherical clusters, and cylinders occur in three dimensions. Moreover, the particle aggregates can often be arranged to form disordered liquidlike configurations, but also crystallinelike superstructures such as grids of stripes and lamellae, hexagonal lattices of clusters, and bubbles.

In many cases a simple mechanism to explain the microseparation is the competition between short-range attraction, driving cluster aggregation, and long-range repulsion that hinder their growth. For colloidal systems, the short-range attraction can be due to depletion forces and van der Waals forces, while the longer-range repulsion stems from dipolar forces as in Langmuir monolayers and ferrofluids, or from partially screened electrostatic forces. For sufficiently strong long-range repulsion, the standard vapor to liquid transition is inhibited in favor of microseparation. These systems have been intensively studied by theoretical [10,22–24] and numerical approaches [25–29]. The nonequilibrium rheological properties of microseparated systems are particularly interesting, since the response can be solidlike or liquidlike responses depending on the length and time scales, or the applied shear stress, which can considerably modify the patters. For example, experiments show that sheared aqueous foams act as elastic solids for small deformations and flow for large applied shear [30,31]. Cluster phases in colloidal systems become dilatant under flow [32,33] as commonly observed in granular media. Finally in Ref. [34] the role of geometrical confinement in the shearing of colloidal systems is considered.

A useful theoretical framework to interpret the rheological properties of microseparated systems is that of the jamming transition [35]. A solidlike or liquidlike response can be considered as signatures of different phases separated by a transition controlled by density, temperature, or stress. In the jammed phase particles and clusters cannot move freely because of mutual interactions or internal constraints and the system behaves like a solid. When the temperature is raised or when the stress exceeds the yield value, particles overcome the trapping barriers and are able to flow like a liquid. While jamming phase diagrams can be obtained experimen-

tally [36], the precise nature of the transition is still not completely understood theoretically. The dynamics of a system near the jamming transition is very intermittent as shown experimentally in Ref. [37] for a single layer of bubbles floating on a liquid surface, and in foam simulations [38–40]. Stain bursts are typical in the plastic deformation of amorphous solids, as shown in numerical simulations [41–43], but also of microscale crystals [44,45] where they are due to the collective dynamics of dislocations [46,47].

In this paper we present results of numerical simulations on the rheology of two-dimensional colloidal microphases in confined geometries. We consider an ensemble of colloidal particles interacting by a potential with short-range attraction and long-range repulsion. As a function of the density and depending on the constraints imposed by the confinement, the colloidal system displays a variety of equilibrium microphases, such as clusters, stripes, or bubbles [48]. Here, we analyze the behavior of the system when a shear profile is imposed on the fluid. In particular, we focus on the stability of the pattern morphology under shear, especially in the intermediate high-density region which has not been studied so far. The rheological behavior of the system is dependent on the density and on the corresponding microphase. At low densities, the colloidal particles separate into clusters that are easily sheared. In this case we observe that shearing is assisted by cluster rotations, a process that is reminiscent of the shear of granular media [49]. At higher densities the colloidal particles form stripes. When the stripes are oriented parallel to the shear direction, the system deforms easily, following the imposed velocity profile. On the other hand, when the stripes are oriented perpendicular to the shear direction the system tends to jam. Only under the application of sufficiently high shear rate is the system able to flow. This is done by a reorientation of the stripes along the shear direction. Similarly, bubble phases are jammed at low shear rates and flow at large shear rate. In order to flow, the bubbles tend to coalesce into stripes which are then easily sheared. The possibility to control, modify, and stabilize a specific pattern is particularly appealing for the technology of new materials. From this point of view, the application of shear stress could represent a promising strategy to control the structure of microphases.

This paper is organized as follows. First we describe the microscopic model of the system and its equilibrium properties, in the bulk and under confinement, in Sec. II A; then the rheological quantities as well as the simulations details are introduced in Sec. II B. Then in Secs. III–V, respectively, we describe the rheological properties for the cluster, the stripe, and the bubble phases. In particular, for each case we discuss the shear rate profile as a function of time, the flow curve (that is, the stress-strain curve), and the velocity profile of the particle aggregate as a function of the distance from the confining walls. In Sec. VI, we discuss the effect of thermal fluctuations on the rheology. A comparison of the behavior of the fluid under shear, adopting different pattern morphologies, is drawn in Sec. VII.

II. THE MODEL

A. Equilibrium

Within the framework of the competing interactions, we consider a bidimensional fluid, in which the effective potential for a pair of colloidal particles is

$$U_{pp}(r) = \begin{cases} A\left(\frac{\sigma}{r}\right)^n - \frac{\epsilon_a \sigma^2}{R_a^2} \exp\left(-\frac{r}{R_a}\right) + \frac{\epsilon_r \sigma^2}{R_r^2} \exp\left(-\frac{r}{R_r}\right) & \text{if } r \leqslant R_{\text{cut}}, \\ 0 & \text{otherwise}, \end{cases} \tag{1}$$

r being the interparticle distance and σ the particle diameter. Such a potential is characterized by a soft-core repulsive term at very short distances, followed by an attractive well plus a repulsive hump at larger distances (see Fig. 1, upper panel). The potential parameters are $n=12$, $A=0.018$ for the short-range repulsion, $R_a=1\sigma$, $\epsilon_a=1$ for the short-range attraction, and $R_r=2\sigma$, $\epsilon_r=1$ for the longer-range repulsion. The short-range repulsion takes into account the impenetrability of the particles, while the remaining part of the potential mimics the colloid interaction mediated by the surrounding fluid. The potential is truncated at $R_{\text{cut}}=10\sigma$. With the present choice of the parameters, the minimum of the potential is located at $r\sim\sigma$, while the maximum value of the longer-range repulsive hump is at $r\sim 4\sigma$.

The interaction potential of Eq. (1) is similar to those studied in [10,12,23] for three-dimensional systems. Other commonly employed potentials are modifications of the Derjaguin-Landau-Verwey-Overbeek (DLVO) [50,51] potential describing screened charges. The general features of the system, such as the pattern morphologies and their rheological properties, should not depend on the precise choice of the potential, provided it displays competing interactions. In case of two-dimensional fluids our model is the same as the one discussed in [27,48], but for the short-range repulsion which is treated as a hard core in the latter, while it is implemented as a soft-core potential in the present work. This difference is not particularly important from the point of view of the general features of the phase diagram in bulk, which is schematically depicted in Fig. 1 (bottom panel). At sufficiently low temperature, the present model supports the passage from droplets to stripes to bubbles as the density increases. The main difference from the bulk model studied in [27] is merely an overall shift of the phase diagram toward lower densities.

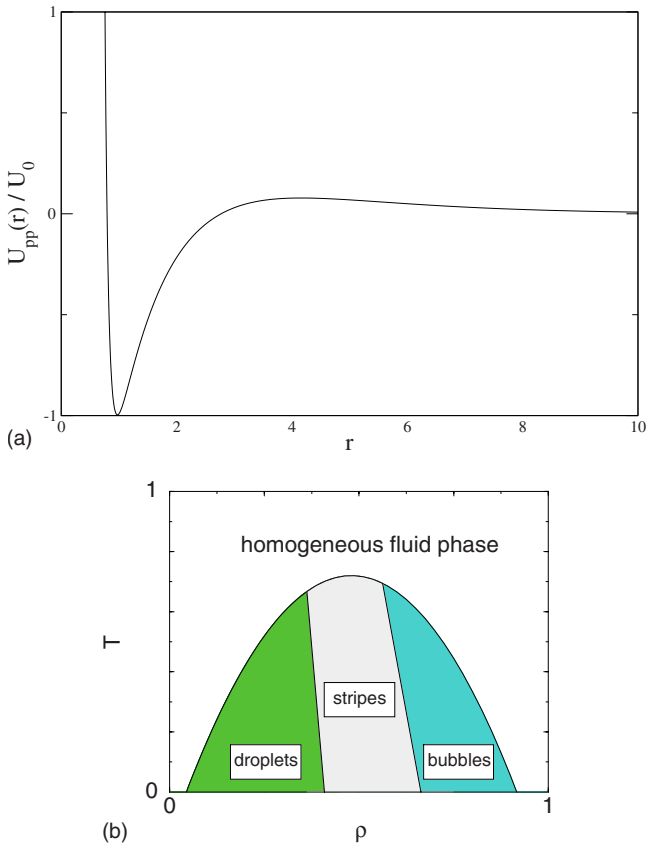

FIG. 1. (Color online) Upper panel: Particle-particle effective potential corresponding to Eq. (1), in units of the potential well depth $U_0=|U_{pp}(r=\sigma)|$. Bottom panel: Schematic phase diagram, in the density-temperature plane (ρ,T) for a bulk bidimensional fluid subject to competing interactions.

In our model, the fluid is confined along the x direction by smooth parallel walls, the separation of which is L_x. The wall-particle interaction is treated as a rather steep potential of the form

$$U_{\mathrm{WP}}(x) = C \exp(-x/\xi), \tag{2}$$

where x is the distance from the wall. The parameters we use in simulations are $\xi=0.1\sigma$ and $C=U_0$, U_0 being the depth of the attractive well of the particle-particle potential. As the range of the wall-particle interaction is very short and the repulsion very strong, such a potential mimics very well the effects of neutral hard walls, as we have also verified by performing some Monte Carlo simulations with a hard-wall potential too.

Under lateral confinement, if the hard-disk potential is used for the short-range repulsion as in [48], a transition from stripe to clusters occurs as the temperature is lowered. Such a transition disappears in our case, where the soft-core potential repulsion is used. The results discussed in [48] can be obtained if the exponent n of Eq. (1) is increased up to 36. But, as the aim of this work is to study the effect of shear on different pattern morphologies, disregarding at first the thermal noise, the change of morphology with temperature is not of interest at this stage. Moreover, with the present choice of the potential parameters, we are able to study the stripe and bubble phases at relatively lower densities, meaning that we carry out simulations with smaller systems.

In this work we discuss three densities $\rho\sigma^2=0.15,0.3,0.5$, corresponding to the cluster, stripe, and bubble regimes. The clusters and the bubbles are arranged onto a triangular superlattice, so that the particle configurations are specular. One of the goals of our work, in fact, is to study how such a hypothetical symmetry between filled and empty regions in the particle configuration affect the rheology of the fluid. The stripes, instead, form a grid of parallel layers. In each microphase the pattern period is $P\sim 11\sigma$. The crystalline order of the superlattice is signaled by the occurrence of Bragg peaks in the static structure factor at short wave vectors K_p that are roughly connected to the period through the relation $P\approx 2\pi/K_p$. The random phase approximation for this kind of potential has provided predictions in good agreement with simulations [27]. The maximum size for the particle aggregates, instead, is dominated by the width of the attractive well of the particle-particle potential. Thus, in the present case, we see that cluster diameter is $\sim 4\sigma$, similar to the bubble diameter and the stripe width.

The addition of a geometrical constraint, such as the presence of neutral walls along one of the directions, is a source of further frustration for the system, mainly if the wall separation L_x is not commensurate with the intrinsic bulk periodicity. For our model, the most peculiar case is represented by the striped phase, where the alignment of the stripes depends strongly on the value of L_x. In particular, if $L_x=mP+\Delta_s$ (m is an integer and Δ_s the stripe width), the stripe orientation is parallel to the walls, otherwise we observe the formation of a mixed phase with two parallel stripes next to the walls and stripes perpendicular to the walls in the center of the slit. In Fig. 2, typical configurations for different patterns between walls are plotted. Such configurations are generated through Monte Carlo simulations in the canonical ensemble (NVT, N number of particles, V volume, T temperature). In our simulations N ranges from 1000 to 2000 particles, and the temperature is equal to $T=0.4U_0$.

B. Rheology

To simulate the rheology of the colloidal system, we consider a simple overdamped dynamics for the particles under the action of an external force field due to the shear. A moving colloidal particle in a fluid is subject to a drag force. In particular, for a spherical particle of radius a moving at small velocity v, the drag force is given by $F_d=-\Gamma v$, with $\Gamma=6\pi\eta a$ where η is the fluid viscosity. In this paper, we apply a weak linear shear profile to the carrier fluid $\vec{V}(x)=V_0 x\hat{y}/L_x$ and, correspondingly, the colloid particle is subject to a drag force profile $\vec{F}_d(x)=F_0 x\hat{y}/L_x$, where $F_0=\Gamma V_0$. Neglecting inertial and thermal effects, the equation of motion for the particles is given by:

$$\Gamma\frac{d\vec{r}_i}{dt} = \vec{F}_d(x) + \sum_j \vec{f}_{pp}(\vec{r}_j - \vec{r}_i), \tag{3}$$

where the interparticle forces are computed from the potential in Eq. (1),

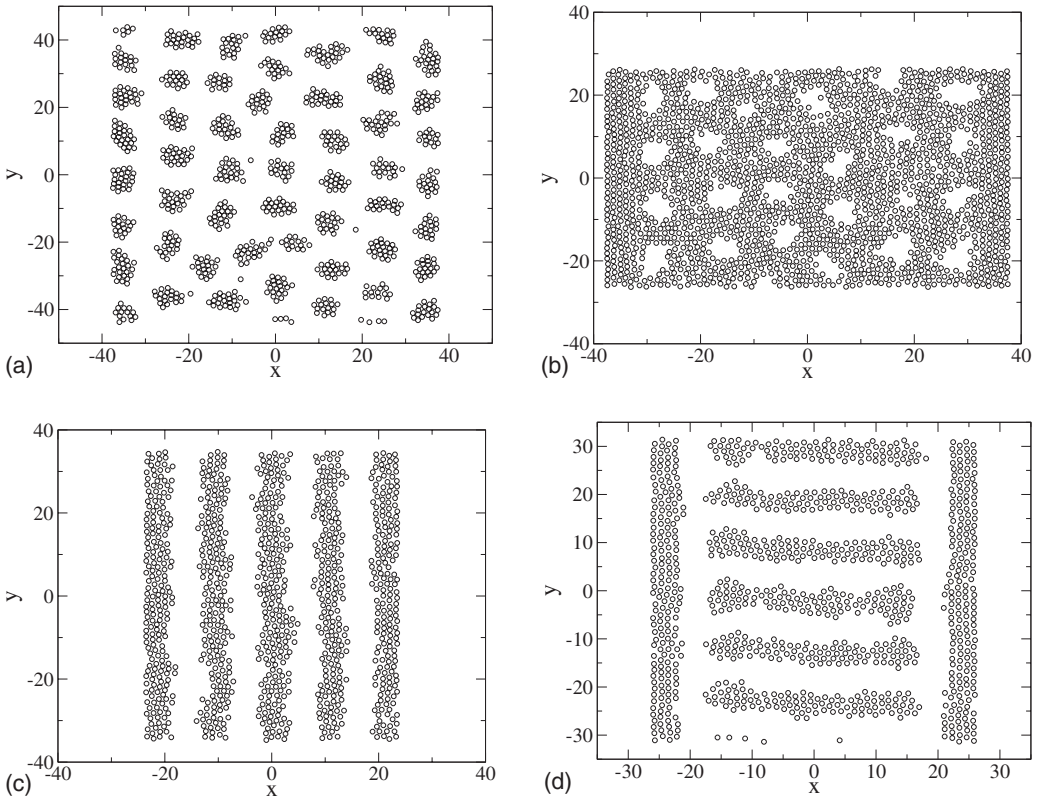

FIG. 2. Typical configurations obtained via Monte Carlo simulations for different densities and different values of the wall separation L_x, and $T=0.4U_0$. In particular, we show configurations obtained for $\rho=0.15\sigma^2$ and $L_x=76\sigma$ (top left), $\rho=0.5\sigma^2$ and $L_x=76\sigma$ (top right), $\rho=0.3\sigma^2$ and $L_x=48\sigma$ (bottom left), and $\rho=0.3\sigma^2$ and $L_x=53\sigma$ (bottom right). When the wall separation L_x is not commensurate with the stripe period, the perpendicular alignment is favored over the parallel one.

$$\vec{f}_{pp}(\vec{r}) = -\frac{\partial U_{pp}}{\partial \vec{r}}. \tag{4}$$

In the present study, we do not consider hydrodynamic interactions which can be important for sheared colloidal particles, although strong confinement is expected screen long-range effects. Equation (3) is integrated numerically by means of an adaptive step-size fourth-order Runge-Kutta algorithm. In the present simulations, we fix the time scales, setting $\Gamma=1$. Equilibrium configurations obtained from Monte Carlo simulations at $T=0.4U_0$ are first relaxed at $T=0$ in absence of external forces, integrating Eq. (3) for $F_0=0$. Then we apply an external shear profile to the resulting configurations and study the system as a function of F_0 and ρ. Thermal fluctuations can also be introduced in the model by adding a Gaussian random force $\vec{\eta}_i(t)$ to Eq. (3). The correlations of the random force are given by

$$\langle \vec{\eta}_i(t)\vec{\eta}_j(t')\rangle = 2\Gamma T\delta_{ij}\delta(t-t'). \tag{5}$$

Most of the simulations are performed at $T=0$ and we discuss the effect of temperature in Sec. VI.

It will be instructive to compare the internal shear strain rate with the externally imposed strain rate $\dot{\gamma}_{\rm ext} \equiv \frac{1}{2}\frac{\partial V_y}{\partial x} = V_0/(2L_x)$. The internal strain rate is in general not uniform and it is necessary to consider its average value defined as

$$\langle \dot{\gamma} \rangle = \frac{2}{L_x}(\langle v_y^+ \rangle - \langle v_y^- \rangle), \tag{6}$$

where $\langle v_y^{\pm} \rangle$ is the y component of the particle velocity restricted to the $x \gtrless 0$ domain. To obtain a clearer picture of the internal strain rate, in order to quantify the deviations from a laminar flow, we measure the particle velocity profile $\langle v_y(x)\rangle$ dividing the system into n_s strips oriented along y and averaging the y component of the velocities of the particles in each strip. In particular, we use $n_s=7$ for $L_x=76$ and $n_s=5$ for $L_x=48,53$. Finally, we measure the stress-strain curves of the system computing the internal shear stress as (see Chap. 4 of Ref. [52])

$$\sigma_{xy} = -\frac{1}{L_x L_y}\sum_{ij}(x_i - x_j) f_{pp}^{(y)}(\vec{r}_i - \vec{r}_j). \tag{7}$$

In the present simulations, we choose a set of parameters that allow us to explore the different microphases. We have not explored entirely the parameter space, although we expect that the qualitative features of the rheological behavior do not depend strongly on the parameters and on the way the system is confined. We have tested that the confinement does not have a strong effect if the structures are sufficiently wide. Varying the confinement size L_x at constant density in the cluster or in the bubble phase does not have a large effect as long as at least three layers (of clusters, stripes, or bubbles) are present.

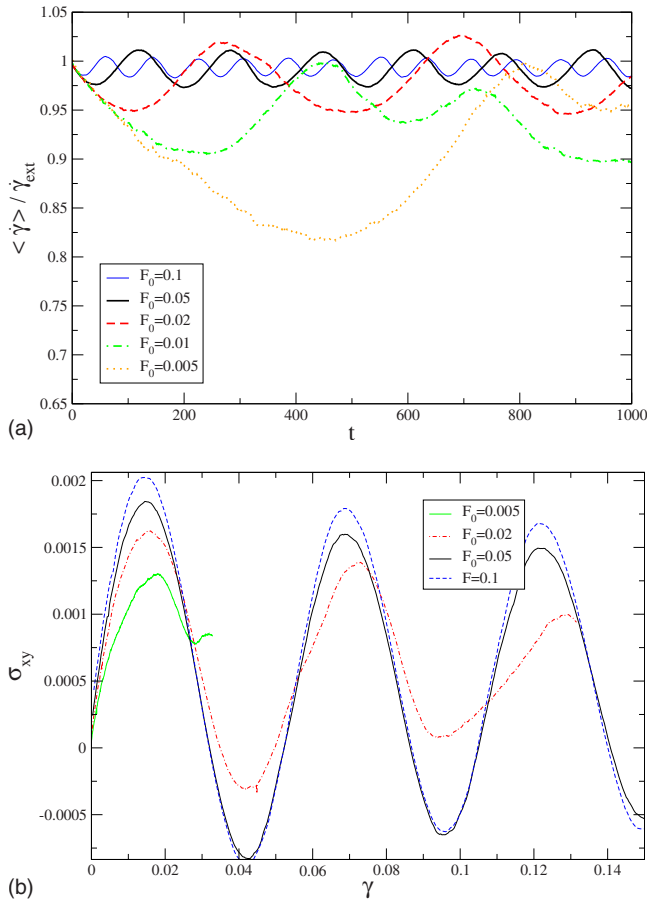

FIG. 3. (Color online) Upper panel: The average strain rate, divided by the external strain rate $\dot{\gamma}_{\text{ext}} \equiv V_0/(2L_x)$, as a function of time for different values of F_0 for a system with $N=1000$, $\rho=0.15$, and $L_x=76$. Bottom panel: The stress-strain curves for the same cases shown in the upper panel.

III. CLUSTER PHASE

The rheological properties of the cluster phase are ruled by the interactions between individual clusters. At low temperatures individual particles inside the clusters do not move, thus the clusters can be considered as rigid objects which repel each other. In Fig. 3 (upper panel) we report the average strain rate $\dot{\gamma}$ of the system normalized by the external strain rate. The average strain rate shows characteristic oscillations, which are a peculiarity of the pattern geometry: at low temperatures the clusters arrange into a regular superlattice and to flow the system must overcome a Peierls-Nabarro periodic potential. In other words, the oscillations are connected to the sliding past of clusters moving along adjacent columns. The period of the oscillations diminishes as the external applied force F_0 increases, as the clusters move faster. Oscillations are also present in the stress-strain curves as shown in Fig. 3 (bottom panel). For the time scales and shear rates that we have studied, we see a slowing down of the dynamics at low F_0 but the system does not jam. We would expect that at very low F_0 jamming would still occur because a yield stress is needed to overcome effective Peierls-Nabarro in the superlattice formed by the clusters.

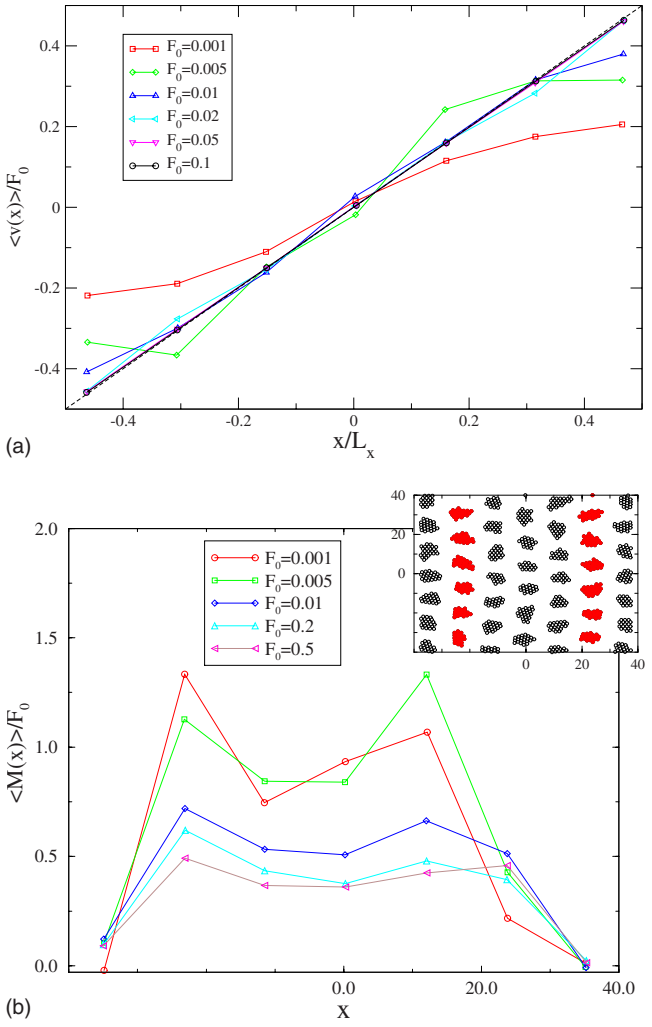

FIG. 4. (Color online) Upper panel: The velocity profiles for different values of F_0, for a system with $N=1000$, $\rho\sigma^2=0.15$, and $L_x=76\sigma$. Notice the deviation from the externally imposed linear profile (dashed line) occurring at low shear rates. Data are averaged over time and over ten realizations. Bottom panel: The torque M profiles acting on the clusters. In the inset we show a typical configuration of the system.

Nevertheless, we could not simulate efficiently a similar regime as the relaxation time becomes too long.

In Fig. 4 (upper panel) we show the velocity profile of the clusters. The external applied velocity profile is also shown as a dashed line. At low F_0 the velocity profile shows that the colloid particles are slower with respect to the surrounding medium. Increasing the external force, instead, the colloid velocity profile tends to be equal to the external one (dashed line). In particular, as F_0 increases, the velocity profile tends to be linear at first in the middle of the box and then nearby the walls. Hence the flow appears to be laminar in the middle of the box, while slippage can be present close to the walls.

We see that the cluster lattice is distorted by the shear deformation and clusters in different columns have to slide past each other. This process is occasionally helped by rotations around the clusters center of mass. Due to the shear profile individual clusters are subject to a net torque that can induce rotations, creating a sort of roller-bearing effect [54].

Similar rotations are commonly observed in the shear of granular media and is very important in earthquakes when the faults are filled by a granular gouge [49]. Similarities between colloidal systems and granular media have been pointed out on the basis of rheological measurements in Ref. [32]. Here, we measure the average torque of the clusters as a function of the horizontal coordinate of their center of mass. As can be seen in Fig. 4 (bottom panel), the torque displays a characteristic pattern depending on the cluster position. The clusters nearby the walls rotate less than the rest because the interaction with the surrounding clusters is limited on one side; the central clusters, instead, are those for which the applied velocity is less important as most of the particles experiment an almost zero drag velocity, so that their rotation is essentially due to the repulsion with the clusters flowing in the nearby columns. Finally the clusters whose position is intermediate between the walls and the center of the simulation box, experiment both the effects due to the applied drag force and to the cluster-cluster repulsion, so that the net torque is the highest.

IV. STRIPE PHASES

When we consider the rheology of the stripe phase, we have to pay attention to the orientation of the stripes with respect to the shear direction. By slightly tuning L_x we can obtain configurations in which the stripes are all parallel to the walls or mixed configurations made up of two stripes parallel to the walls, while in the middle they arrange perpendicularly to the walls.

The most interesting case is that corresponding to the perpendicular stripes. In fact, at low forces the system jams, failing to reorient in the flow direction. Hence, for $F_0 < 0.03$, the average strain rate is lower than the external rate, while for larger F_0 their ratio tends to 1 (see Fig. 5, upper panel). This behavior is reflected by the stress strain curve (Fig. 5, bottom panel), which changes character for $F_0 \geqslant 0.03$ where the yield stress is followed by a strain-rate weakening part while, for $F_0 < 0.03$, the stress reaches a plateau. The peak stress for low F_0 scales in a viscous manner as $\sigma_p \simeq C\dot{\gamma}$ and changes character for $F_0 > 0.03$ scaling as $\sigma_p \simeq \sigma_Y + C'\dot{\gamma}$, with $C' < C$ (inset of Fig. 5). We also note strong fluctuations in the high-strain regime, a behavior that is often observed in systems with avalanchelike flows as in [40–43,46,47,53].

The jamming of the system is clearly visible in the velocity profiles, where we see that the central part of the system has zero velocity and only the two boundary parallel stripes are flowing (Fig. 6, upper panel). Typical snapshots of the system, when it is jammed and when it is flowing are plotted in the bottom panels of Fig. 6 too [54].

The case of parallel stripes is particularly simple to shear. The velocity profile rescaled to the applied force is always linear for each value of F_0 we have used. The most interesting aspect is perhaps the behavior of the stress-strain curves which shows some fluctuations, even if much more smaller than those observed with perpendicular stripes, and probably due to the irregularity in the stripe surfaces (see Fig. 7). The mean stress is a linear function of the strain rate, indicative

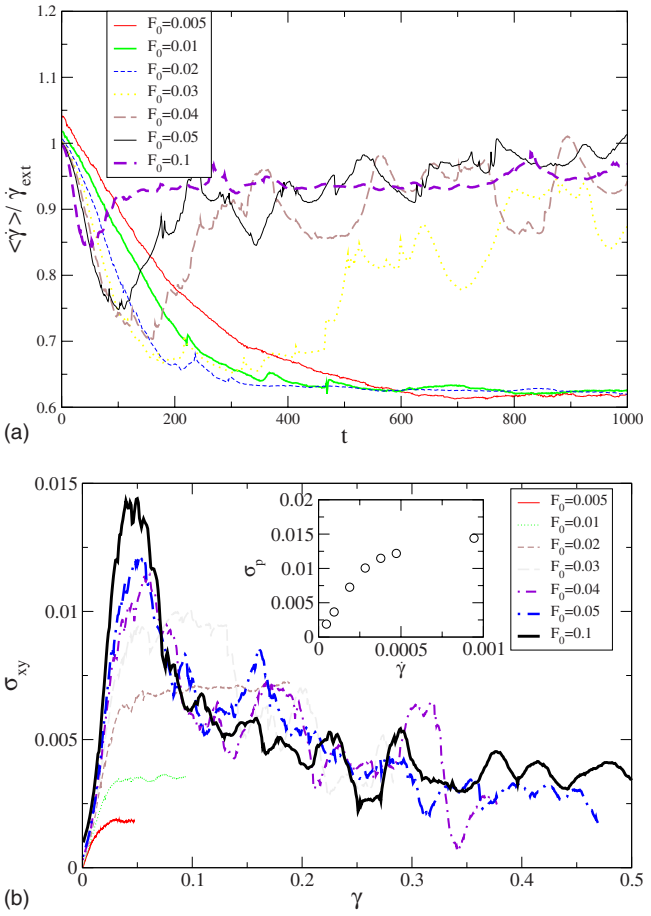

FIG. 5. (Color online) Upper panel: The average strain rate as a function of time for different values of F_0 for a system with $N=1000$, $\rho=0.3$, and $L_x=53$ plotted in log-linear scale. In the initial condition the stripes are mostly perpendicular to the flow direction. Bottom panel: The stress-strain curves. In the inset we report the maximum stress σ_p as a function of the strain rate $\dot{\gamma}$. Notice the change of behavior as the systems yields at higher rates.

of a simple viscous behavior. An extrapolation at low shear rate would indicate a very low yield stress of the order of $\sigma_Y \simeq 10^{-5}$.

V. BUBBLE PHASES

Increasing the density, the system develops a bubble phase in which the bubbles are arranged on a triangular superlattice. From a qualitative point of view, the bubbles under shear become more and more elongated along the direction of the applied velocity field, until they join to form stripelike configurations (bottom panel of Fig. 9). The rheology of the bubble phase has some similarities with that of the perpendicular stripe phase, since both phases jam at low shear rates. The main difference with respect to the stripe phase is that, for small external applied strain, the bubble phase is completely jammed. This is evident from the slowing down of the average strain rate for $F_0 \leqslant 0.005$ (Fig. 8 upper panel) and also from the velocity profile which is completely flat (Fig. 9 upper panel). In the case of perpendicular stripes, instead the jamming involves only the central region,

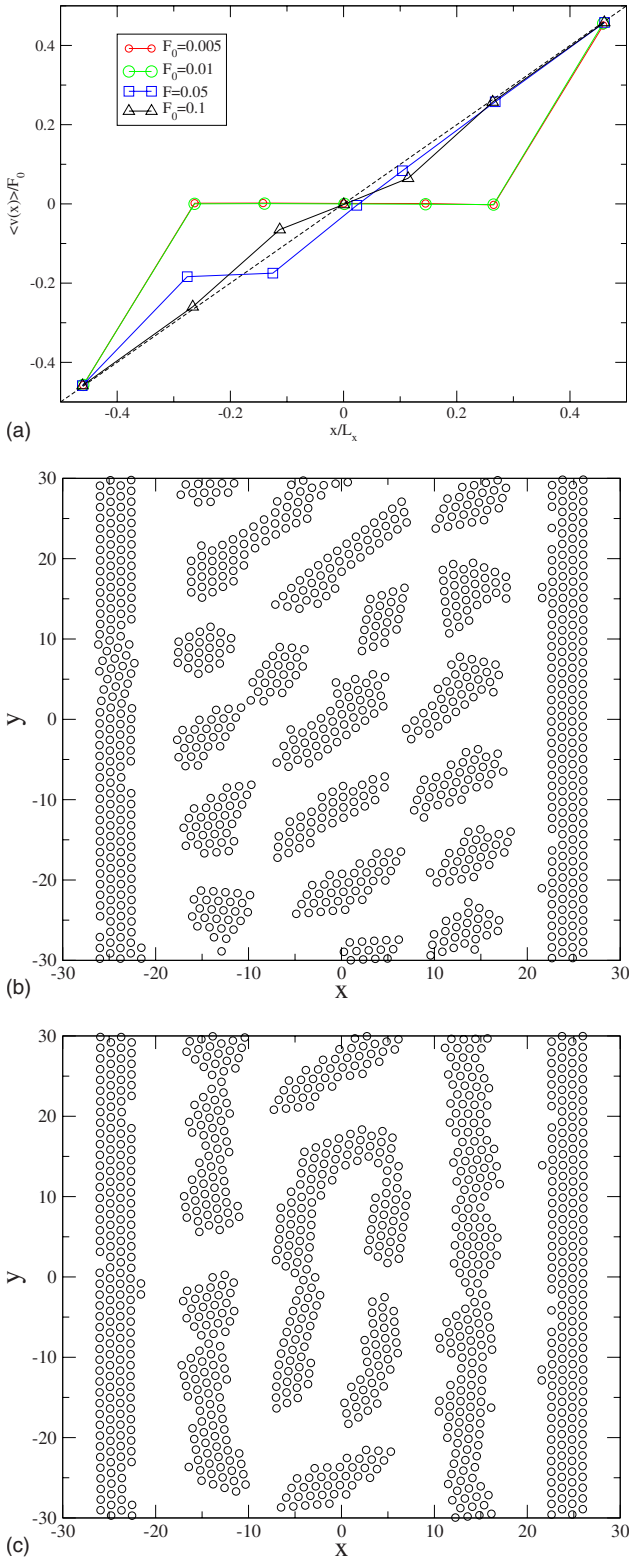

FIG. 6. (Color online) Velocity profiles as a function of time for different values of F_0, for a system with $N=1000$, $\rho=0.3$, and $L_x=53$. At low shear rate only the outer (parallel) stripes moves while the perpendicular stripes are jammed. At higher shear rate the perpendicular stripes break and flow. The dashed line represents the imposed profile. In the bottom panels, particle configurations for $F_0=0.1$ (middle) at the yield point, when the central stripes break at $F_0=0.1$ and (bottom) at high strain $\gamma=1$.

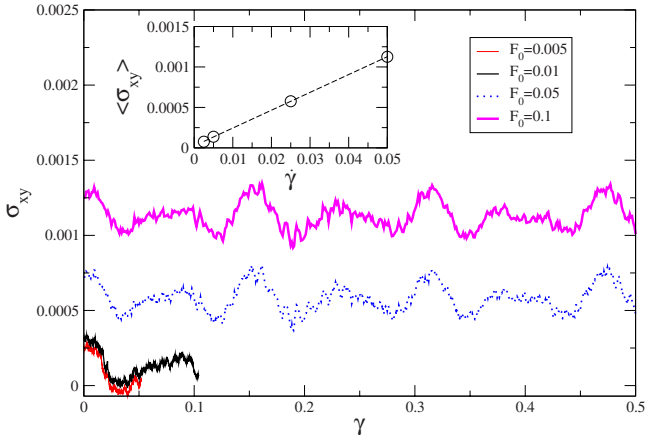

FIG. 7. (Color online) Stress-strain curves for different values of F_0 for a system with $N=1000$, $\rho=0.3$, and $L_x=48$. The initial state is characterized by stripes which are all parallel to the walls and to the flow direction.

while the stripes close to the walls flow as well.

When the applied force to the bubble phase is greater than the peak stress, the system starts to flow and once again parallel stripes are formed (Fig. 9 bottom panel), since this state is the easiest to shear [54]. The peak stress is an increasing function of the strain rate as depicted in the inset of the bottom part of Fig. 8. Extrapolations at low shear rate suggest a yield stress of the order $\sigma_Y=0.02$. The shear weakening observed in the stress-strain curve is reminiscent of the stripe phase, but the yield stress σ_Y measured in the bubble phase is about an order of magnitude greater than that observed in the stripe case. This is easily understandable as, in the bubble phase, the particles are strongly packed together, so that the motion of the individual particles is hindered by the surrounding ones. In other words, collective motion of particles is necessary to ensure a structural change of the system. We notice as well that the stress-strain curve is characterized by large fluctuations, suggesting again intermittent and abrupt rearrangements as commonly observed in plasticity [44–47] and in foam rheology [38–40].

In order to better understand the yielding of the bubble phase, we perform a Voronoi triangulation of the particle system and follow the evolution of the topological defects. Due to the $T=0$ condition, the system is locally ordered with a few topological defects around the bubbles. As the system is sheared, we observe the nucleation and propagation of dislocations, corresponding to pairs of fivefold and sevenfold coordinated atoms [54]. In particular, dislocations are sometimes created at the surface of a bubble and then propagate toward the nearest bubble (see Fig. 10). Hence, we can see the shear-induced transformation from bubbles to stripes as a ductile fracture process: the system first deforms plastically in the vicinity of the bubbles and eventually a crack propagates, leading to the coalescence of the bubbles into stripes.

It is also interesting to compare the rheology of the bubble phase with the one of the cluster phase. At equilibrium, the cluster phase and the bubble are characterized by configurations which are specular. Under shear, however, the clusters are easily sheared also for very low values of F_0, while a yield stress must be overcome in the bubble phase. More-

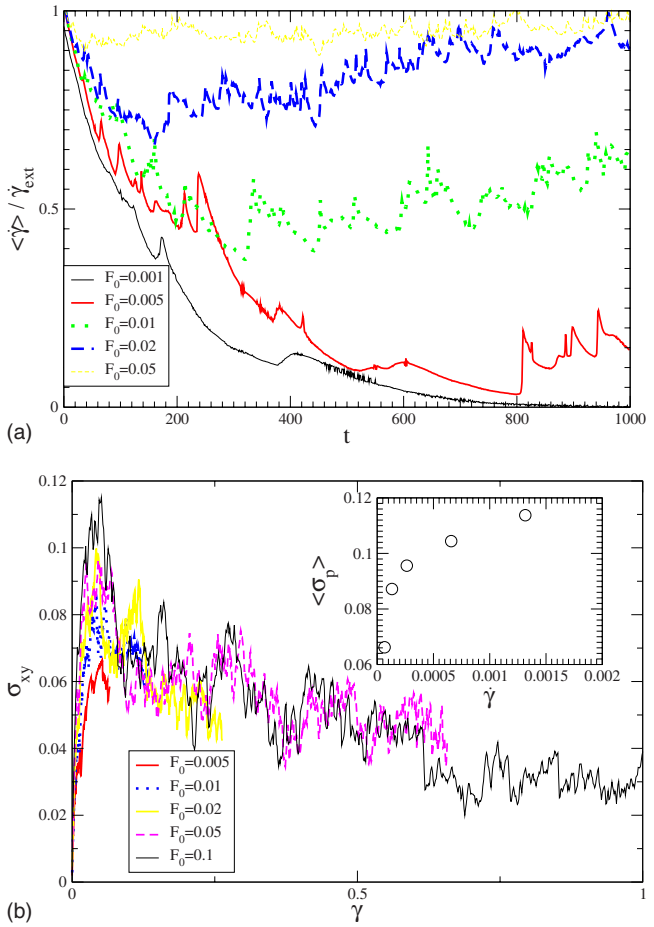

FIG. 8. (Color online) Upper panel: The average strain rate as a function of time for different values of F_0 for a system with $N=2000$, $\rho\sigma^2=0.5$, and $L_x=76\sigma$ plotted in log-linear scale. Notice that at large F_0 the strain rate reaches a steady value, while for $F_0=0.0001$ the strain rate decreases toward zero, indicating a jammed phase. Bottom panel: The stress-strain curves for different values of F_0. In the inset we show the peak stress as a function of the applied strain rate $\dot{\gamma}$.

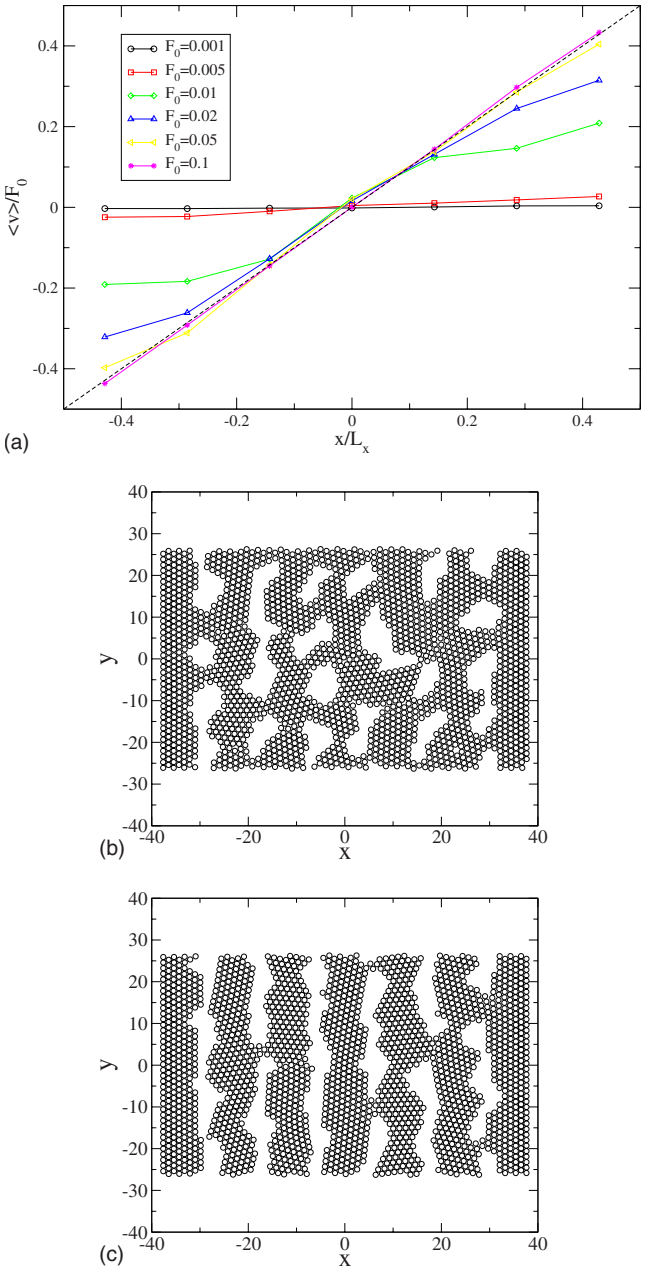

FIG. 9. (Color online) Upper panel: The velocity profiles for different values of the drag force F_0 for a system with $N=2000$, $\rho\sigma^2=0.5$, and $L_x=76\sigma$. Data are averaged over time and over ten realizations. Notice the deviation from the externally imposed linear profile occurring at lower shear rates. For $F_0=0.0001$, the system is jammed and the profile is flat. Bottom panels: Subsequent snapshots for the system at $F_0=0.1$. The snapshots are taken at the yield strain (middle) and at large strain (bottom). Notice the crossover from bubble to stripes at large strains.

over, while the clusters rotate and maintain their shape until F_0 is rather large, the bubbles deform almost immediately. Notwithstanding these large differences in the structure of the systems, the velocity profiles appear to be very similar for $F_0>0.005$. In particular the velocity profiles obtained in the bubble phase are similar to those obtained in the cluster phase but with smaller external forces. Moreover, the velocity profiles tend to become linear at first in the middle of the box simulation and eventually near the walls.

VI. THERMAL FLUCTUATIONS

All the numerical simulations discussed in the previous section have been performed at $T=0$. This is not a realistic condition for most colloidal systems where thermal agitation is provided by the interactions with fluid molecules. On the other hand, simulations at $T=0$ allow us to define the reference state for the flowing system, providing the limit case to be observed at low temperature. In order to test the robustness of the rheological properties, we include thermal fluctuations in the model. We can expect that temperature could be particularly relevant for jammed configurations that can be destroyed by thermally activated motion, while at high shear rate thermal fluctuations should not change the rheological properties.

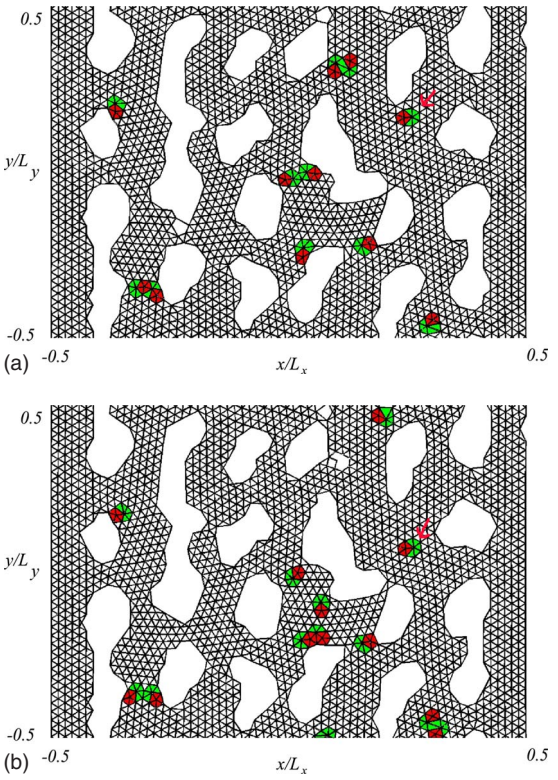

FIG. 10. (Color online) Voronoi triangulations of the configuration of the system configurations at two subsequent time steps for a system with $N=2000$, $\rho=0.5$, $L_x=76$, and $F_0=0.1$. The snapshots are taken around the yield strain $\gamma \simeq 0.11$. Pairs of sevenfold and fivefold particles form dislocations and are colored, respectively, in green (light gray) and red (dark gray). For clarity, we do not show the topological defects arising at the sample boundary and around the bubbles. Notice the motion of a dislocation between neighboring bubbles (indicated by an arrow).

To test this general picture, we consider the case of perpendicular stripes at low shear rates ($\rho\sigma^2=0.3$, $L_x=53$, $F_0=0.01$). As discussed in Sec. IV, the system would be jammed at $T=0$ with the central perpendicular stripes that are unable to move. As we increase the temperature beyond $T^* \simeq 0.15U_0$, the system undergoes a transition to a flowing phase, as demonstrated by the changes in the velocity profiles shown in Fig. 11(a). The transition is reflected by a change in morphology, since the stripes are reoriented in the flow direction (see the lower panels of Fig. 11). A signature of the transition can be seen also in the stress-strain curve reported in Fig. 12(a). In particular, the average internal shear stress σ_{xy} is found to decrease rapidly for $T>T^*$ [see the inset of Fig. 12(a)], which is indicative of the reorientation of the stripes along the shear direction reducing the stress. Next we consider the case of high shear rate $F_0=0.1$, where the perpendicular stripes yield already at $T=0$ and reorient in the flow direction. At $T>0$ the rheology is similar, but the reorientation is assisted by thermal fluctuations. As a consequence of this the peak stress in the stress-strain curve decreases with temperatures, indicating that the system becomes softer [see Fig. 12(b)].

Finally, we investigate the role of temperature in the bubble phase. Also in this case thermal fluctuations make the

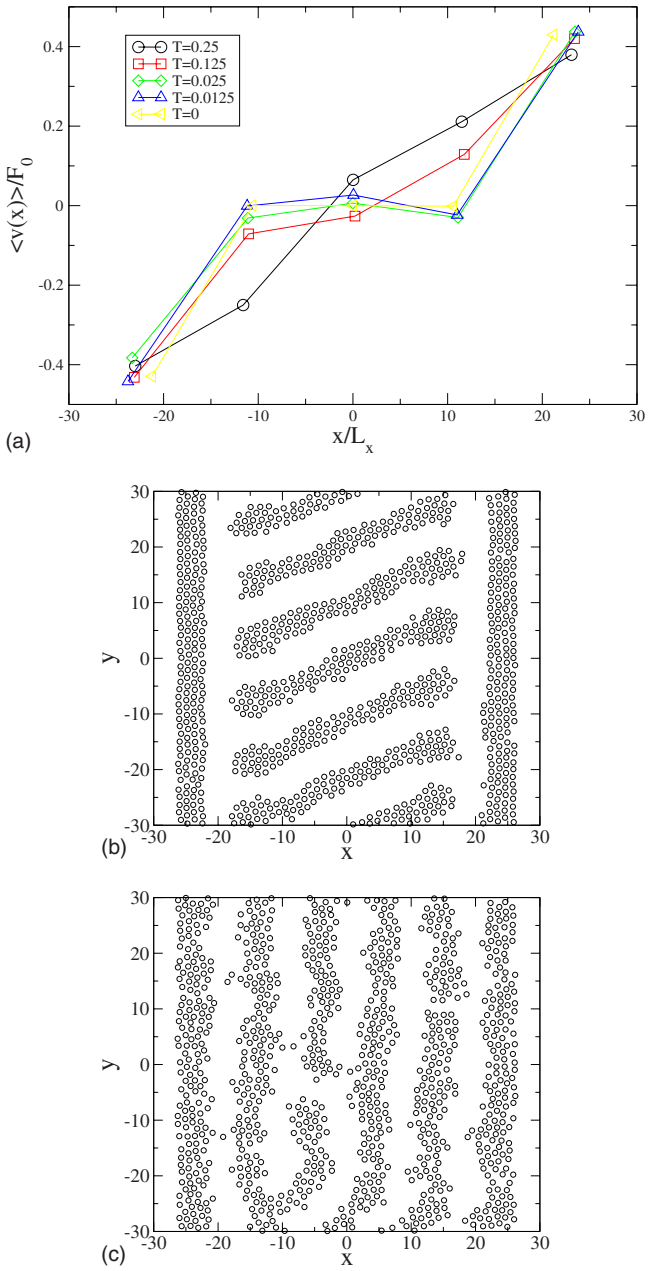

FIG. 11. (Color online) Upper panel: The velocity profiles as a function of temperature for different values of F_0, for a system with $N=1000$, $\rho=0.3$, $F_0=0.01$, and $L_x=53$. At low temperature we recover the $T=0$ behavior, with moving outer (parallel) stripes and jammed perpendicular stripes. At higher temperature the perpendicular stripes break and reform parallel stripes. Bottom panels: particle configurations at different temperatures: $T=0.0125U_0$ (middle) and $0.25U_0$ (bottom).

system more ductile. At $T=0$, the bubbles first deform elastically and eventually break up, forming stripes. When thermal fluctuations are present, dislocation nucleation at the boundary of the bubbles is enhanced and plastic flow is favored over brittle fracture. Hence, at sufficiently high temperature, the system is able to flow without deforming the bubble shape just by creating dislocations [54].

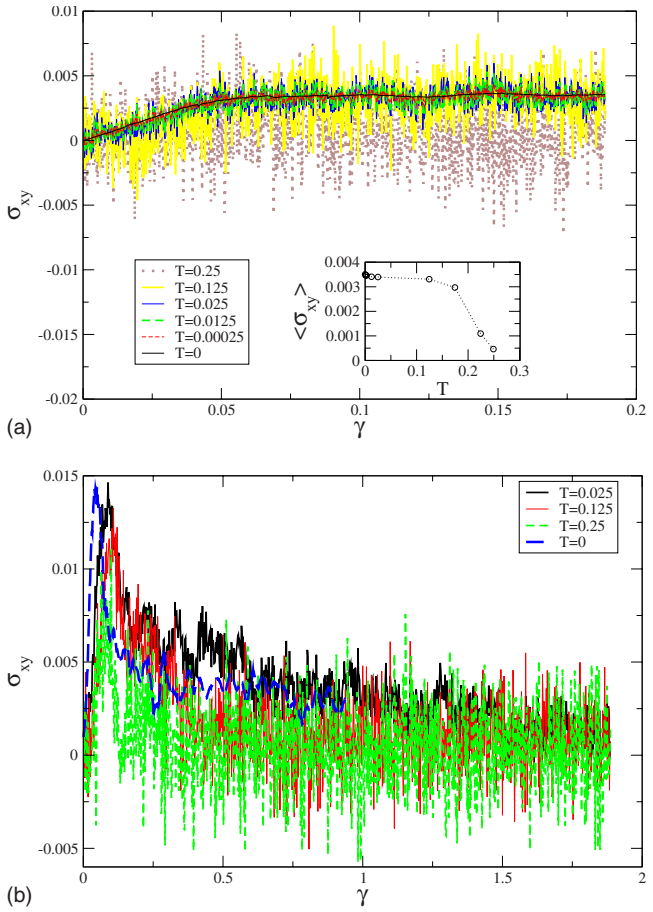

FIG. 12. (Color online) Stress-strain curves for different values of T for a system with $N=1000$, $\rho=0.3$, and $L_x=53$. The initial state is characterized by stripes which are all parallel to the walls and to the flow direction. (a) Simulations at low shear rate ($F_0=0.01$). Thermal fluctuations lead to a reorientation of the stripes for $T>0.15U_0$. This is reflected in a rapid decrease of the internal shear stress, as reported in the inset. (b) Simulations at $F=0.1$. The peak stress decreases with temperature, indicating a softening of the stripes that reorient more easily in the flow direction.

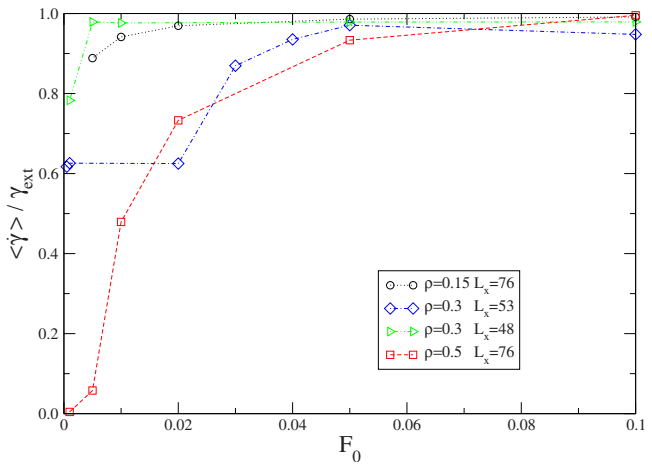

FIG. 13. (Color online) Average strain rate, divided by the external strain rate $\dot{\gamma}_{\text{ext}} \equiv V_0/(2L_x)$, as a function of the external force F_0 for different pattern morphology at equilibrium. The cluster case corresponds to $\rho=0.15\sigma^2$, $L_x=76\sigma$, the parallel stripes to $\rho=0.3\sigma^2$, $L_x=48\sigma$, the perpendicular stripes to $\rho=0.3\sigma^2$, $L_x=53\sigma$, and the bubble case to $\rho=0.5\sigma^2$, $L_x=76\sigma$.

VII. DISCUSSION AND CONCLUSIONS

In this paper, we have studied the rheological properties of a model for colloidal particles with competing interactions. In particular, we concentrated on the morphological changes induced by shear on the equilibrium microphases. At sufficiently high densities, the ideal configuration for shear is the one with stripes parallel to the flow direction. When the strain rate is not strong enough to transform the existing microphase into stripes, the system tends to jam. This behavior is observed both in systems with perpendicular stripes and with bubbles. At lower densities, we have observed a cluster phase that is easily sheared with the help of cluster rotations.

To summarize the behavior of the system at different densities, we compare the strain rate obtained for different pattern morphologies. In particular, the strain rate is averaged over time and normalized with respect to the externally applied strain, in order to quantify the discrepancy with respect to a laminar flow. The results, as a function of the applied external force F_0, are plotted in Fig. 13. For each pattern we see that, for sufficiently high values of F_0, the flow is laminar, that is the ratio $\langle\dot{\gamma}\rangle/\dot{\gamma}_{\text{ext}}$ tends to unity. For smaller values of the drag forces, the behavior of the systems is rather different and strictly dependent on the equilibrium configuration. In particular the cluster phase is easy to shear. In this case the system is never jammed for the values of F_0 we have used, suggesting that if a yield stress exists, it is very small. When the system is already arranged on stripes parallel to the walls, the flow is laminar even for the lowest values of F_0. In the case of perpendicular stripes the strain rate profile is characterized at first by a plateau, which is connected to the coexistence of the flowing stripes nearby the walls and the jammed central stripes. Then at $F_0 \geqslant 0.03$ the stripes breaks and tend to rearrange in the flow direction. Finally in the bubble phase, the system is at first completely jammed as it demonstrated by the zero value of the ratio $\langle\dot{\gamma}\rangle/\dot{\gamma}_{\text{ext}}$. It seems, however, that in case of perpendicular stripes, the partial jamming persists on a wider range of F_0 with respect to the bubble phase. Finally we observe that in the cases in which the system undergoes a structural change, such as that from the perpendicular alignment of stripes to the parallel one, or from the melting of the bubble phase to reform parallel stripes, a peak occurs in the strain-stress curve. The height of such a peak in the bubble phase is greater than the corresponding one in the stripe phase by an order of magnitude. Moreover, strong fluctuations appear in the stress-strain curve, which might suggest similarities with systems in which avalanchelike rearrangements occur.

The rheological behavior discussed above has been obtained at $T=0$. It is thus important to discuss which features are expected to persist when thermal effects are taken into account. We can expect that, if the temperature is below the melting transition, the behavior observed at high shear rates should be independent of the temperature. At low shear rates,

however, close to the jamming transition, thermal fluctuations could help overcome the geometrical constraints leading to a slow creep deformation. We have tested these ideas by simulating parallel stripes and bubbles at low shear rates. We have observed that above a critical temperature the system, which would be jammed at $T=0$, is able to flow. This is expected from general considerations on jamming phase diagrams, that usually depend on stress, density, and temperature [35]. At high density, in the bubble phase, thermal fluctuations lead to a more ductile deformation of the microstructure that can flow without deforming the bubbles.

ACKNOWLEDGMENTS

S.Z. acknowledges the financial support of the European Commission NEST Pathfinder program TRIGS under Contract No. NEST-2005-PATH-COM-043386. We thank A. Parola for useful discussions.

[1] M. Klokkenburg, R. P. Dullens, W. K. Kegel, B. H. Erné, and A. P. Philipse, Phys. Rev. Lett. **96**, 037203 (2006).
[2] W. Gelbart, R. Sear, J. Heath, and S. Chaney, Faraday Discuss. **112**, 299 (1999).
[3] F. Elias, C. Flament, J. Bacri, and S. Neveu, J. Phys. I **7**, 711 (1997).
[4] F. Ghezzi and J. Earnshaw, J. Phys.: Condens. Matter **9**, L517 (1997).
[5] M. Seul and D. Andelman, Science **267**, 476 (1995).
[6] F. Bardi, C. Cametti, and S. Sennato, Colloids Surf., A **306**, 102 (2007).
[7] P. J. Lu, J. C. Conrad, H. M. Wyss, A. B. Schofield, and D. A. Weitz, Phys. Rev. Lett. **96**, 028306 (2006).
[8] A. Stradner, H. Sedwick, F. Caedinaux, W. Poon, S. Egelhaaf, and P. Schurtenberger, Nature (London) **432**, 492 (2004).
[9] M. F. Islam, K. H. Lin, D. Lacoste, T. C. Lubensky, and A. G. Yodh, Phys. Rev. E **67**, 021402 (2003).
[10] F. Sciortino, S. Mossa, E. Zaccarelli, and P. Tartaglia, Phys. Rev. Lett. **93**, 055701 (2004).
[11] P. Charbonneau and D. R. Reichman, Phys. Rev. E **75**, 011507 (2007).
[12] A. de Candia, E. Del Gado, A. Fierro, N. Sator, M. Tarzia, and A. Coniglio, Phys. Rev. E **74**, 010403(R) (2006).
[13] T. Hoare and R. Pelton, J. Phys. Chem. B **111**, 1334 (2007).
[14] M. Hecht, J. Harting, and H. J. Herrmann, Phys. Rev. E **75**, 051404 (2007).
[15] S. Reynaert, P. Moldenaers, and J. Vermont, Langmuir **22**, 4936 (2006).
[16] J. Caballero, A. Puertas, A. Fernandez-Barbero, and F. J. de las Nieves, Colloids Surf., A **270-271**, 285 (2005).
[17] A. I. Campbell, V. J. Anderson, J. S. van Duijneveldt, and P. Bartlett, Phys. Rev. Lett. **94**, 208301 (2005).
[18] J. Goldman, S. Andrews, and D. Bray, Eur. Biophys. J. **33**, 506 (2004).
[19] A. Szabo, E. D. Perryn, and A. Czirok, Phys. Rev. Lett. **98**, 038102 (2007).
[20] K. Kern, H. Niehus, A. Schatz, P. Zeppenfeld, J. Goerge, and G. Comsa, Phys. Rev. Lett. **67**, 855 (1991).
[21] S. Muller, P. Bayer, C. Reischl, K. Heinz, B. Feldmann, H. Zillgen, and M. Wuttig, Phys. Rev. Lett. **74**, 765 (1995).
[22] D. G. Barci and D. A. Stariolo, Phys. Rev. Lett. **98**, 200604 (2007).
[23] M. Tarzia and A. Coniglio, Phys. Rev. E **75**, 011410 (2007).
[24] D. Pini, G. Jialin, A. Parola, and L. Reatto, Chem. Phys. Lett. **327**, 209 (2000).
[25] C. J. Olson Reichhardt, C. Reichhardt, and A. R. Bishop, Phys. Rev. Lett. **92**, 016801 (2004).
[26] C. Reichhardt, C. J. Olson, I. Martin, and A. R. Bishop, Europhys. Lett. **61**, 221 (2003).
[27] A. Imperio and L. Reatto, J. Chem. Phys. **124**, 164712 (2006).
[28] A. D. Stoycheva and S. J. Singer, Phys. Rev. E **65**, 036706 (2002).
[29] R. Larson, J. Chem. Phys. **96**, 7904 (1992).
[30] A. D. Gopal and D. J. Durian, Phys. Rev. Lett. **75**, 2610 (1995).
[31] A. D. Gopal and D. J. Durian, Phys. Rev. Lett. **91**, 188303 (2003).
[32] D. Lootens, H. van Damme, Y. Hemar, and P. Hebraud, Phys. Rev. Lett. **95**, 268302 (2005).
[33] C. Osuji, C. Kim, and D. Weitz, e-print arXiv:0710.0042.
[34] I. Cohen, T. G. Mason, and D. A. Weitz, Phys. Rev. Lett. **93**, 046001 (2004).
[35] A. J. Liu and S. R. Nagel, Nature (London) **396**, 21 (1998).
[36] V. Trappe, V. Prasad, L. Cipelletti, P. Segre, and D. Weitz, Nature (London) **411**, 772 (2001).
[37] J. Lauridsen, G. Chanan, and M. Dennin, Phys. Rev. Lett. **93**, 018303 (2004).
[38] D. J. Durian, Phys. Rev. E **55**, 1739 (1997).
[39] S. Tewari, D. Schiemann, D. J. Durian, C. M. Knobler, S. A. Langer, and A. J. Liu, Phys. Rev. E **60**, 4385 (1999).
[40] T. Okuzono and K. Kawasaki, Phys. Rev. E **51**, 1246 (1995).
[41] C. Maloney and A. Lemaître, Phys. Rev. Lett. **93**, 016001 (2004).
[42] M. J. Demkowicz and A. S. Argon, Phys. Rev. B **72**, 245206 (2005).
[43] N. P. Bailey, J. Schiøtz, A. Lemaître, and K. W. Jacobsen, Phys. Rev. Lett. **98**, 095501 (2007).
[44] M. D. Uchic, D. M. Dimiduk, J. N. Florando, and W. D. Nix, Science **305**, 986 (2004).
[45] D. M. Dimiduk, C. Woodward, R. LeSar, and M. D. Uchic, Science **312**, 1188 (2006).
[46] M.-C. Miguel, A. Vespignani, S. Zapperi, J. Weiss, and J.-R. Grasso, Nature (London) **410**, 667 (2001).
[47] F. Csikor, C. Motz, D. Weygand, M. Zaiser, and S. Zapperi, Science **318**, 251 (2007).
[48] A. Imperio and L. Reatto, Phys. Rev. E **76**, 040402(R) (2007).
[49] J. A. Astrom, H. J. Herrmann, and J. Timonen, Phys. Rev. Lett. **84**, 638 (2000).
[50] B. V. Derjaguin and L. Landau, Acta Physicochim. URSS **14**, 63 (1941).
[51] E. J. Verwey and J. T. G. Overbeek, *Theory of the Stability of Lyophobic Colloids* (Elsevier, Amsterdam, 1948).

[52] J. H. Weiner, *Statistical Mechanics of Elasticity* (Wiley, New York, 1983).
[53] M. Tsamados, A. Tanguy, F. Leonforte, and J. Barrat, Eur. Phys. J. E **26**, 283 (2008).
[54] See EPAPS Document No. E-PLEEE8-78-026808 for animations of the following: the shear of the cluster phase, the shear of the perpendicular stripe phase showing the reorientation of the stripes at the yield point, the shear-induced stripe formation in the bubble phase, the Voronoi triangulations of the configurations in the sheared bubble phase, and the evolution of the Voronoi triangulation at $F_0=0.01$ and $T=0.125U_0$. For more information on EPAPS, see http://www.aip.org/pubservs/epaps.html.